ORIGINAL ARTICLE

Effect of solvent exchange on the properties of carbon xerogel and carbon xerogel/polypyrrole composites for supercapacitors

Meryem Samancı[1] · Elif Daş[2,3] · Ayşe Bayrakçeken Yurtcan[1,2]

Abstract

Carbon xerogels (CXs) with three-dimensional (3D) structure, unusual surface, physical, electrical and mechanical properties and their electrically conductive polymer polypyrrole (PPy) composites were synthesized as electrode materials for supercapacitors. The effect of different resorcinol/formaldehyde (R/C) ratios, whether solvent exchange with or without acetone and polypyrrole addition on the physicochemical (FTIR, XRD, BET, SEM and TGA) and electrochemical properties (CV, 1000 cycles) of the synthesized materials were investigated. It was observed that the R/C ratio and the solvent exchange process prior to drying affect the specific surface areas and the pore size distributions, thereby positively affecting the specific capacitance. PPy film thickness was observed to be effective in the specific capacitance of the electrode in PPy composite synthesis. Among the synthesized materials, the highest specific capacitance values belong to polypyrrole/carbon xerogel composites. As a result of the analysis and calculations, it was found that the highest specific capacitance belongs to CX2/PPy composite with 599 Fg^{-1} at 5 mVs^{-1}. CX2/PPy composite has been found to have a capacitance retention rate of 80.30% at the end of 1000 cycles.

Keywords Carbon xerogel · Polypyrrole composites · Ambient drying · Solvent exchange · Specific capacitance · Supercapacitor

1 Introduction

Rapid population growth and technological developments in recent years cause the depletion of the energy resources used and the increase of environmental pollution. Therefore, the importance of effective, efficient and reliable use of energy is increasing day by day in energy technologies and sustainable energy systems. This increases the importance of using and developing energy storage systems. In order for the electrochemical energy storage to be at maximum levels, importance is given to studies on subject such as higher energy density, lower cost, longer life and improved material sustainability. Supercapacitors (also known as electrochemical capacitors or ultra-capacitors) represent a class of energy storage devices that can store electrical energy converted from various energy sources [1, 2].

The performance of a supercapacitor is largely determined by the electrode performance. Supercapacitors are examined in three groups according to the electrode material used. The electrodes used are, carbon materials, transition metal oxides [3, 4] and conductive polymers [5] and utilization of both [6, 7]. The electrode materials of EDLC have been widely used as carbon materials with high electrical conductivity, high surface area, with controlled surface morphology, good corrosion resistance and thermal stability, good processability, abundance and low cost of production [8]. Carbon-based materials make easy capacitive double-layer formation and also provide a high surface area skeleton that enhances contact between the accumulated pseudocapacitive materials and the electrolyte. Recently, researchers combined physical (non-faradaic reaction) and chemical (faradaic reaction) charge storage mechanisms into a single electrode by combining carbonaceous materials with conductive polymers (CP) [9, 10] and metal oxides [11, 12] by synthesizing composite electrodes (hybrid capacitors).

✉ Ayşe Bayrakçeken Yurtcan
ayse.bayrakceken@gmail.com

1 Faculty of Engineering, Department of Chemical Engineering, Atatürk University, 25240 Erzurum, Turkey

2 Department of Nanoscience and Nanoengineering, Atatürk University, 25240 Erzurum, Turkey

3 Department of Physics, Atatürk University, 25240 Erzurum, Turkey

Electrically CP electrodes, for electrochemical super-capacitors, such as polyaniline (PANI) [13], polypyrrole (PPy) [14], polythiophene (PTh) [15], polyethenedioxy-thiophene (PEDOT) [16] and derivatives have been studied by researchers (pseudocapacitors) due to the presence of various oxidation structures (doped state), high capacitive energy density and low material cost materials. Among the conductive polymers, PPy is a commonly used one and there are large number of researches for the application of PPy as supercapacitor material in recent years. Because PPy has high electrical conductivity in the doped state, high specific capacitance (easy up to 100 Fg^{-1}) and good chemical and thermal stability, particularly easy synthesis and environmental friendliness [17].

By combining polypyrrole with graphene oxide [18], with carbon nanotubes [19], polyaniline with carbon aerogel [20], PEDOT with graphene and polythiophene with graphene [21], polyaniline with graphene oxide [22] and 3D reduced graphene oxide with polyaniline [23], the researchers have synthesized composite electrodes for the utilization in supercapacitors.

Carbon aerogels (supercritical drying) [24], carbon cryogels (freeze drying) [25] and carbon xerogels (ambient drying), which are three-dimensional form of carbon materials, have advantageous properties such as high surface area, low thermal conductivity, high acoustic resistivity. These open cell foam structures are obtained from wet gels. This is generally prepared by the sol–gel method [26]. In supercritical drying and freeze drying processes, it is aimed to minimize surface tensions and pore shrinkage rates caused by capillary forces applied to the pores at the liquid–vapor interface during drying. However, both supercritical drying and freeze-drying are time-consuming, costly and hard to use. In this instance, solvent exchange is used to reduce capillary forces causative for collapse of the pore wall. In ambient conditions, solvent is exchanged with a liquid with low surface tension before drying. Indeed, 3D carbonaceous materials can be obtained by direct drying and pyrolysis of aqueous resorcinol–formaldehyde (RF) gels, provided that the synthesis parameters are chosen correctly [27, 28]. Some researchers have shown in their studies that the structure of the RF wet gel can be protected with minimal shrinkage at ambient pressure [29]. Li et al. found that the specific capacitance of xerogel obtained as a result of drying under ambient conditions was 110.06 Fg^{-1} [30]. Lee and colleagues found that the specific capacitance of synthesized carbon xerogel was 81 Fg^{-1} [31].

In this study, carbon xerogels (CX) were synthesized by polycondensation of resorcinol (R) and formaldehyde (F) by changing two different reactant concentrations. The preparation of carbon xerogels was followed by two routes after the sol–gel process; (1) solvent exchange with acetone (2) without solvent exchange followed. This processes were followed by atmospheric drying and pyrolysis for both routes. In the second stage, PPy/carbon xerogel composite structures were synthesized by in-situ oxidative chemical polymerization of pyrrole over carbon xerogels. By adding polypyrrole to these four different xerogels synthesized, the superior properties of carbon xerogels and conductive polymers have been tried to be combined. Changes in the physicochemical (FTIR, XRD, BET, SEM, TGA) and electrochemical (CV) results of the composite electrodes were examined.

2 Experimental

2.1 Preparation of resorcinol–formaldehyde wet gels

Sol gel solutions were prepared by using base catalyst. Parameters such as solution pH, monomer concentrations and catalyst affect the density, surface area, particle size and pore size distribution of the materials [32]. Molar ratios of the reactants for resorcinol–formaldehyde xerogels (RFXs) synthesis are given in Table 1. The molar ratios of resorcinol (99%, Sigma-Aldrich) to sodium carbonate (Sigma-Aldrich) (R/C) and resorcinol to water (R/W) were changed and resorcinol to formaldehyde (37%, Sigma-Aldrich), (R/F) ratio was set to a fixed value of 0.5. The Na_2CO_3 catalyst (C) was used to control the pore size and distribution of the wet gels. Using the catalyst, a material having a fine porous structure and a high specific surface area is obtained. Therefore, the R/C ratio in the wet gel is important [30]. First of all, the precursor materials were mixed in the proportions in Table 1. The first pH of the solution was measured to be between 7–7.5. This pH value is a suitable range for gelling to take place [33]. Subsequently, this mixture was cured for 24 h at room temperature. This was followed by gelation at 50 °C for 24 h and at 90 °C for 72 h [34].

Solvent exchanges were carried out in two routes for RF wet gels. In the first route, after the gelation, the samples were left to dry directly at ambient conditions and no solvent exchange is applied. In the second route, after the gelation, the samples were left in acetone (99.5%, Sigma-Aldrich) for 24 h and then again left to dry directly at ambient conditions (Fig. 1a). So that two types of RF wet gels were obtained.

Table 1 Reactant concentrations in the synthesis of carbon xerogels

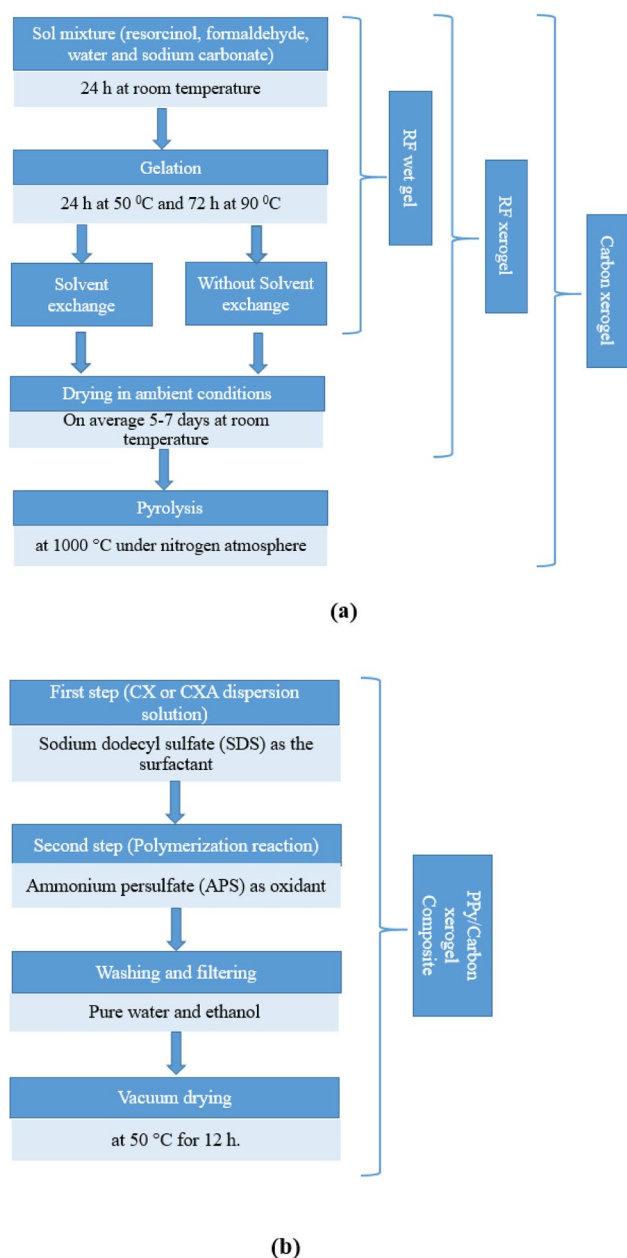| Sample	Resorcinol/formaldehyde (R/F) molar ratio	Resorcinol/water (R/W) molar ratio	Resorcinol/catalyst (R/C) molar ratio
CX1, CXA1	0.5	0.08	100
CX2, CXA2	0.5	0.02	200

(a)

(b)

Fig. 1 **a** Synthesis steps of carbon xerogels (CX, CXA), **b** synthesis steps of PPy/carbon xerogels (CX, CXA)

Acetone is intended to minimize the contraction during the drying of RF wet gels at ambient conditions by providing displacement of acetone with water in the pores due to its low surface tension (20.66 dyne cm^{-1}) and low boiling point (56.5 °C). The surface tension of acetone is approximately one-fourth of the surface tension of water (72.8 dyne cm^{-1}, 20 °C) [35]. As a result of these processes, we can observe how the solvent exchange process using acetone will have an effect on the properties of the synthesized materials.

2.2 Synthesis of carbon xerogel

To obtain carbon xerogels (CX, without solvent exchange or CXA, with solvent exchange in acetone) from RF wet gels, wet gels were pyrolised at 1000 °C under nitrogen atmosphere for 4 h with a heating rate of 15 °Cmin^{-1}. The carbonized RF carbon xerogel was cooled to room temperature in flowing N$_2$ (Fig. 1a). As a result of the carbonization process, a highly porous carbon network structure is obtained by removing excess solvent and volatile components from the structure.

2.3 Preparation of polypyrrole (PPy) composites with carbon xerogel (CX, CXA)

The two main methods of synthesis of conductive polymers are chemical and electrochemical polymerization. The chemical polymerization method, when compared to the electropolymerization method, exhibits an easier and more homogeneous structure [36]. In this study, the synthesis of polypyrrole was made by in situ chemical oxidative polymerization. The composites were prepared as given elsewhere [37]. Briefly, CX or CXA to pyrrole (w/w %98-Aldrich) and ammonium persulfate (98%, Sigma-Aldrich) (APS) to pyrrole ratios were set to 1:2 and 1:1, respectively. Sodium dodecyl sulfate (Sigma-Aldrich, sigmaultra 99%, SDS) was used as the surfactant. 0.1 g corresponding carbon xerogel was mixed in distilled water including SDS, and ultrasonicated for 10 min. Then, stirred for about 2 h below 20 °C. Subsequently, after 5-min refrigeration, pyrrole was added into this solution. Then APS as the oxidant was dissolved in distilled water and then mixed with this solution in order to begin the polymerization reaction and stirred for 2 h under 20 °C. The resulting carbon xerogel/PPy composites were filtered and washed with water and ethanol several times. Finally, obtained composites were dried in vacuum at 50 °C for 12 h (Fig. 1b).

3 Characterization

3.1 Physical characterization

FTIR (Perkin Elmer Spectrum One FT-IR spectrometer) device was used to determine the surface functional groups. Determination of the structural properties of the synthesized samples were obtained by nitrogen adsorption/desorption isotherm analysis with Brunauer, Emmett and Teller (BET) method. Micromeritics 3 Flex 3-port BET surface area and micropore size measuring device were used for surface area. SEM images of prepared carbon xerogels were taken with Zeiss Sigma 300 Instrument and SEM images of PPy composites were taken with Quanta FET 200 Instrument.

X-ray diffractometer (Rigaku Miniflex X-ray diffractometer CuK∞, λ = 15406 Å) was used to analyse the crystal structure in between $5° \leq 2\theta \geq 70°$. Thermal behavior of the materials were analysed by thermogravimetric analyzer (TGA, Netzch STA 400 PC Luxx Thermal analyzer) at a temperature range of 25–1300 °C with a heating rate of 10 °C min^{-1} in an air atmosphere at a flow rate of 60 mlmin^{-1}.

3.2 Electrochemical characterization

Standard three-electrode electrochemical cell system (Pine instrument) connected with a potentiostat (Versastat 3) were used to determine the specific capacitances. Cyclic voltammograms (CVs) were obtained using glassy carbon (GC) electrode, Pt wire and Ag/AgCl electrode as working, counter and reference electrodes, respectively, in 1M sulfuric acid (Merck) electrolyte. An ink composed of water, 1,2-propanediol (Sigma-Aldrich) and 165 μl of Nafion solution (20%, Ion Power, Inc 1.5% wt) were used to prepare the working electrode. The amount of carbon xerogel or carbon xerogel/PPy composite on the electrode was 28 μgcm^{-2}. Fresh and aged electrodes were used for CV experiments. Higher cycles that occur in supercapacitor systems (the continuous charge–discharge state and, therefore, the temperature increase) will cause irreversible undesirable reactions and aging processes on the electrode surface. Fresh and aged electrodes are used in electrochemical tests to study these processes (aging mechanisms) and to improve and enhance the long-term stability of the electrode [38]. Fresh electrode data were recorded after 50 cycles at a scan rate of 50 mVs^{-1} in the potential range of − 0.28–1 V and the aged ones were obtained by cycling the electrode for 1000 cycles. The potential range was changed in between − 0.28 to 0.3, − 0.28 to 0.5, − 0.28 to 0.7, and − 0.28 to 0.9 V potential ranges at a constant scan rate of 50 mV s^{-1}. The scan rate was changed as 5, 20, 50, 100 and 500 mVs^{-1}. Electrochemical impedance spectroscopy (EIS) were used to examine the capacitive and resistive behavior of the carbon xerogels via a potentiostat at 0.4, 0.65 and 0.9 V potentials in 1M H_2SO_4 (Merc) electrolyte at the frequencies in between 0.001 and 100 kHz and got the Nyquist plots for fresh and aged electrodes.

The specific capacitances were calculated from CV curves. The specific capacitances were calculated by the following equation:

$$C_s = \left(\int (I dv)/(vm\Delta V) \right) \qquad (1)$$

where C_S was the specific capacitance, I was the current, V was the potential window, v was the scan rate, m was the mass of carbon xerogel or corresponding composite active material used in the working electrode [37].

4 Results and discussion

Table 2 shows the volumetric shrinkage and mass loss percentages of the synthesized materials. Volumetric shrinkage rates of cylindrical carbon xerogels as a result of ambient drying and pyrolysis were obtained by measuring the narrowing of the diameter by the digital caliper. The mass loss rate before and after pyrolysis of the carbon xerogels were calculated by weighing with precision scales. During drying under ambient conditions, carbon xerogels with an R/C ratio of 100 have less volumetric shrinkage than carbon xerogels with an R/C ratio of 200. The increase in the R/C ratio, in other words, the decrease in the catalyst ratio resulted in an increase in the carbon particle size [39]. In this case, the diameter of the pores also increases. This also explains the decrease in the volume of the micropores and the increase in the volume of the mesopores. This situation is shown in the pore size distribution graphs given in Fig. 4. Since the mesopore walls are wider than the micropore walls, there will be much more precipitation in the mesopores during the drying process due to the surface tension of the solvents in the pore [26, 40, 41]. As a result of these collapses, volumetric shrinkage was higher in CX2 and CXA2 materials during ambient drying. The same volumetric shrinkage occurred in CX1 and CX2 materials during the pyrolysis. On the other hand, CXA1 and CXA2 materials have more volumetric shrinkage than CX1 and CX2. This difference is due to acetone remaining in the pores during the drying after solvent change. In the study of Jun et al. (different R/C, same R/F ratio), the results given in Table 2 were reached as average [42]. The same R/F ratio carbon xerogels after pyrolysis almost gave similar volume shrinkage and mass loss values.

In Fig. 2, FTIR results of the synthesized materials are given. As can be seen from Fig. 2, it is seen that there is no significant change in stretching vibration due to two changes in the R/C ratios. The peaks corresponding to -N bonds were formed with the addition of pyrrole to carbon xerogels which confirmed the successful synthesis of PPy composites due to the polypyrrole originated -N bonds. Peaks between 500 and 1000 cm^{-1} wave numbers indicate the presence of polymerized pyrrole [43]. C–N stretch is available at 1183 cm^{-1}.

Table 2 Shrinkage and mass loss percentages during drying and pyrolysis

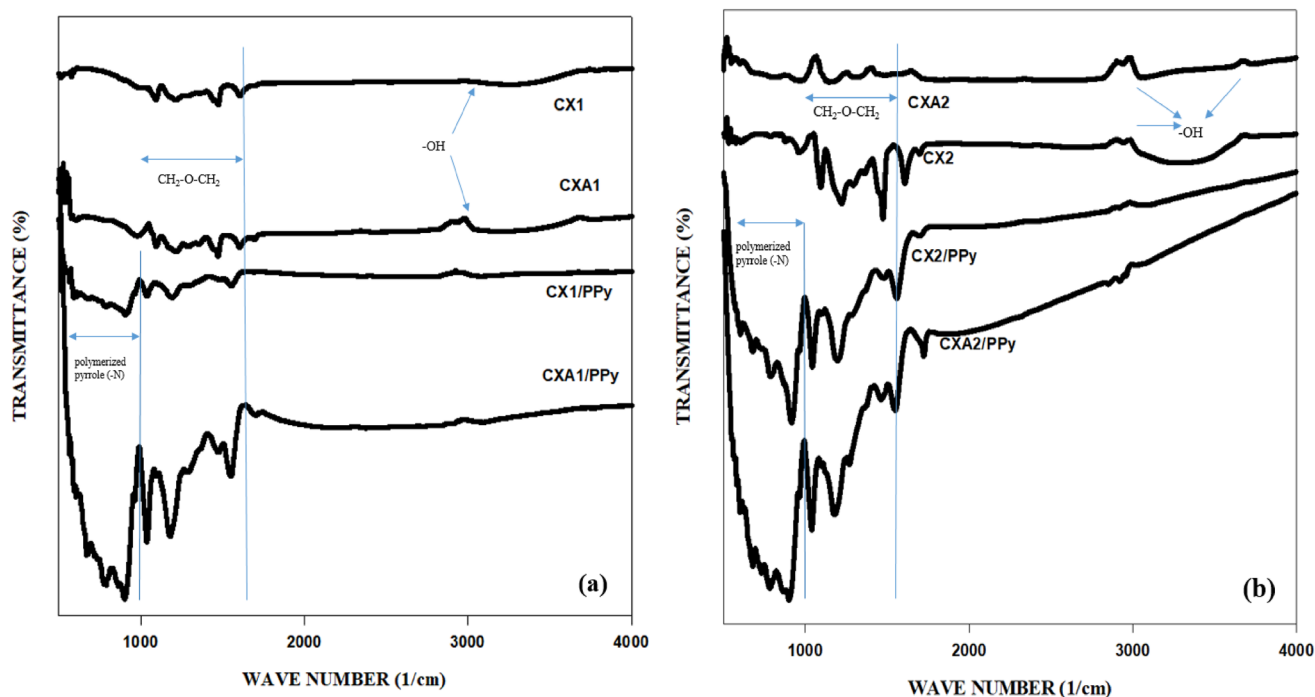| Sample	Volumetric shrinkage after drying (%)	Volumetric shrinkage after pyrolysis (%)	Mass loss during pyrolysis (%)
CX1	28	22	51.5
CXA1	25	26.5	47
CX2	45	23	51.5
CXA2	44	29	56

Fig. 2 FTIR graphs of **a** CXA1, CX1 and their polypyrrole composites, **b** CXA2, CX2 and their polypyrrole composites

Bending of N–H occurred in the wavenumbers of 1705 cm^{-1} and 1730 cm^{-1}. Figure 3a, b shows the peak OH- stretching vibration at 3000 cm^{-1} and 3054 cm^{-1}, respectively. These bonds indicate the presence of hydrogen bonds and adsorbed water in the pores of the carbon xerogels. The absorption peaks of methylene–ether (CH$_2$–O–CH$_2$) (it occurs due to polycondensation) were observed at a few peaks between approximately 1000 cm^{-1} and 1300 cm^{-1} (1050 cm^{-1}, 1298 cm^{-1}, 1368 cm^{-1}). 1482 cm^{-1}, 1500 cm^{-1} wave numbers denote the CH$_2$- and CH$_3$- vibration [30, 44]. C=O and C=C were stretched at around 1690 cm^{-1} and 1725 cm^{-1} [45]. FTIR graphs confirmed that hydroxymethyl derivatives of resorcinol are formed and these derivatives are condensed as methylene bridges. This situation shows that carbon xerogel synthesis takes place with the sol–gel method.
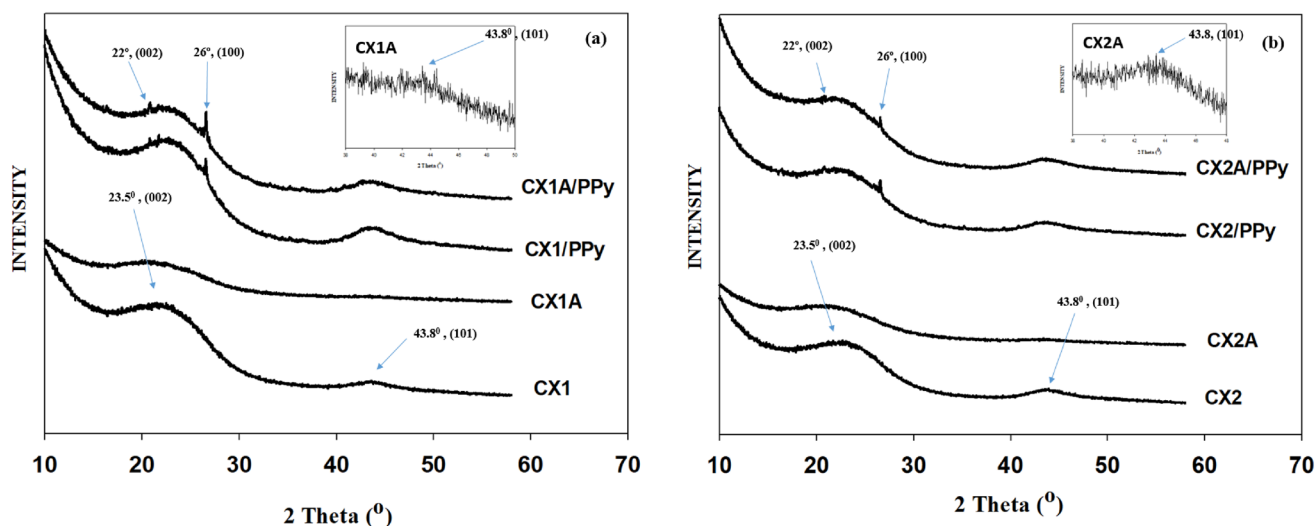

Fig. 3 XRD results of **a** CXA1, CX1 and their polypyrrole composites, **b** CXA2, CX2 and their polypyrrole composites

XRD analysis was carried out to examine the crystal structures of the synthesized materials. XRD graphs of the materials are given in Fig. 3. XRD results showed that carbon xerogels and composites were amorphous. Carbon xerogels show two diffraction peaks at approximately 23.50° and 43.80°, respectively, strong C (002) and weak C (101) at 2θ (Cu K) [30]. The peak located at around 22–23.5° corresponds to C (002) graphitized carbon. The intensity of the peak located at 43.8° shows weak graphitization of C (101). Especially for CXA1 and CXA2 C (101), the peaks are also quite wider. Wide peaks represent irregular carbon structures [18, 46, 47]. Polypyrrole composites give two peaks at approximately 22° and 26°, respectively, corresponding to (002) and (100) peaks [48]. Graphite-like carbon xerogel structures become less prominent by the addition of polypyrrole when forming composites [18].

The pore size distributions, pore volume and N_2 adsorption/desorption isotherms of carbon xerogels and their polypyrrole composites are shown in Fig. 4. According to the International Classification of Pure and Applied Chemistry (IUPAC), isotherms of carbon xerogels exhibit type-IV characteristics, indicating that carbon xerogels are typical mesoporous materials [49]. It shows a hysteresis showing typical H2 characteristics. H2-type hysteresis is also a characteristic of spherical agglomerated systems, but such hysterisating solids do not have to a regular pore size distribution and pore shapes. Polypyrrole composites of carbon xerogels also exhibit type II isotherm characteristics, indicating that carbon xerogels are also mesoporous materials. The hysteresis type also shows a hysteresis showing typical H1 properties representing cylindrical pores [27].

The structural properties of the synthesized materials were determined by BET method. Surface areas, average pore diameters and pore volumes were obtained and given in Table 3. As the R/C ratio increases from 100 to 200, it appears to increase the specific surface area. The highest BET surface area belongs to CXA2 material with 312.3 m^2 g^{-1}. When we look at Table 3, the surface area of the carbon xerogels with solvent exchange with acetone is higher than the carbon xerogels without solvent exchange. In this case, it is seen that precipitation occurs on the pore walls of the carbon xerogels obtained by drying under ambient conditions without acetone (without solvent exchange) under the effect of capillary forces (surface tension of water) [26]. In literature studies, different solvents are used for solvent exchange process. Kraiwattanawong et al. synthesized carbon xerogels with different R/C ratios using ethanol, T-butanol, toluene, water and acetone solvents. They examined the BET surface areas of these synthesized xerogels [50]. By adding polypyrrole to carbon xerogels, the specific surface area of the composites was greatly reduced. This resulted in an increase in average pore diameters. This is due to the fact

that polypyrrole covers the pores of the carbon xerogel structure as a thin film [36].

Surface morphology information of the synthesized materials was determined by SEM images. SEM images of four different carbon xerogel and their PPy composites synthesized according to two different R/C ratios and the presence or absence of solvent exchange with acetone are given in Fig. 5. When we look at the zoomed images of the carbon xerogels, it is observed that the xerogels are in harmony with the BET surface areas. While the CX1, CXA1 and CX2 xerogels have a denser morphology, the 3D porous spherical structure of the CXA2 xerogel is slightly more pronounced. When we look at the studies conducted, xerogel structures tend to be agglomerated as the R/C ratio decreases, and give a more spherical porous structure as the R/C ratio increases [27, 31, 51]. It is clear that PPy loading has taken place on the carbon xerogels. The increase in the R/C ratio increased the density of the PPy spheres on the xerogel surface. Solvent replacement with acetone increased PPy loading in xerogels with the same R/C ratio. BET analysis results also support the morphological structure of the composite surfaces. With the loading of PPy to CXA2 (312.3 m^2 g^{-1}), which has the highest BET surface area, it is seen that there is a more complex network structure of PPy at the surface. It is clear that especially the diameter of PPy spheres coated on CXA2/PPy surface is considerably smaller compared to other PPy composites. This situation shows that the PPy film coating on the surface is more dense than other composites. Since the specific surface areas of xerogels other than CXA2 are close to each other, the morphological images of PPy composites of these xerogels are similar. According to these images, the material with the smallest loading is for CX1/PPy. This situation is explained by the TGA analysis results given in Fig. 6. In addition, some studies have been carried out on the effect of the textural differences of the surface on the structure of the PPy film coating. Babazadeh et al. synthesized PPy/TiO_2 composites using different amounts of TiO_2 by one-step in situ chemical oxidative polymerization method. They have shown that different TiO_2 additives are highly effective on the morphology and textural structure of PPy and PPy/TiO_2 composites. They observed that as the amount of TiO_2 nanoparticles in composites increased, it turned into a nanoparticle-shaped shell in the PPy film coating [52]. Zhu et al. synthesized composites with easy surface-initiated polymerization (SIP) method using PPy and different carbon nanostructures. Depending on the structural properties of carbon nanomaterials, PPy reveals that it has been successfully coated in different forms (roughly or smooth) [53].

Thermogravimetric profiles of carbon xerogels and their PPy composites are given in Fig. 6. In general, little loss of mass was observed in all materials due to moisture loss at low temperatures and removal of organics [18]. Carbon
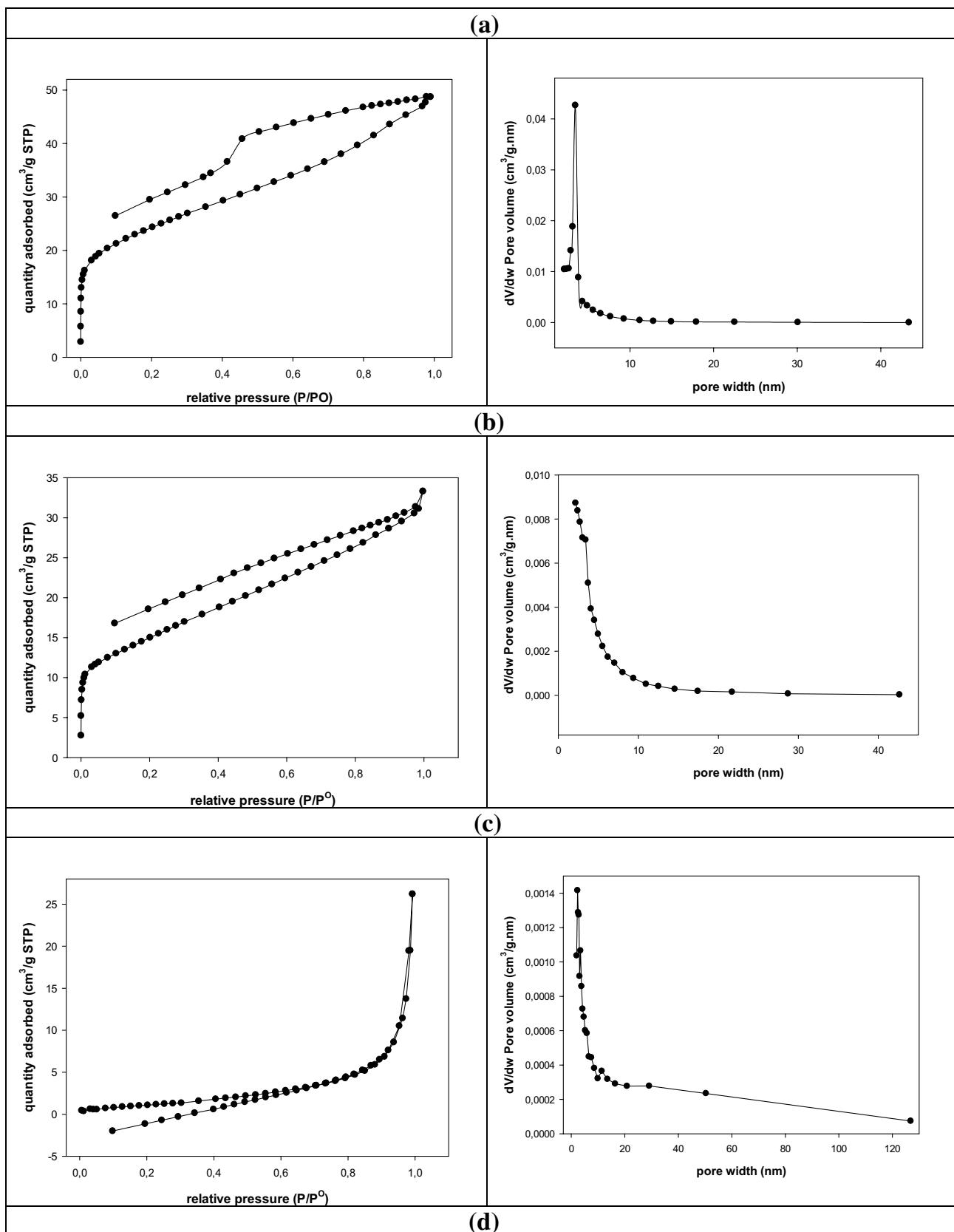
Fig. 4 N_2 adsorption/desorption isotherms and pore size distributions of carbon xerogels and their polypyrrole composites, **a** CXA1, **b** CX1, **c** CXA1/PPy, **d** CX1/PPy, **e** CXA2, **f** CX2, **g** CXA2/PPy, **h** CX2/PPy
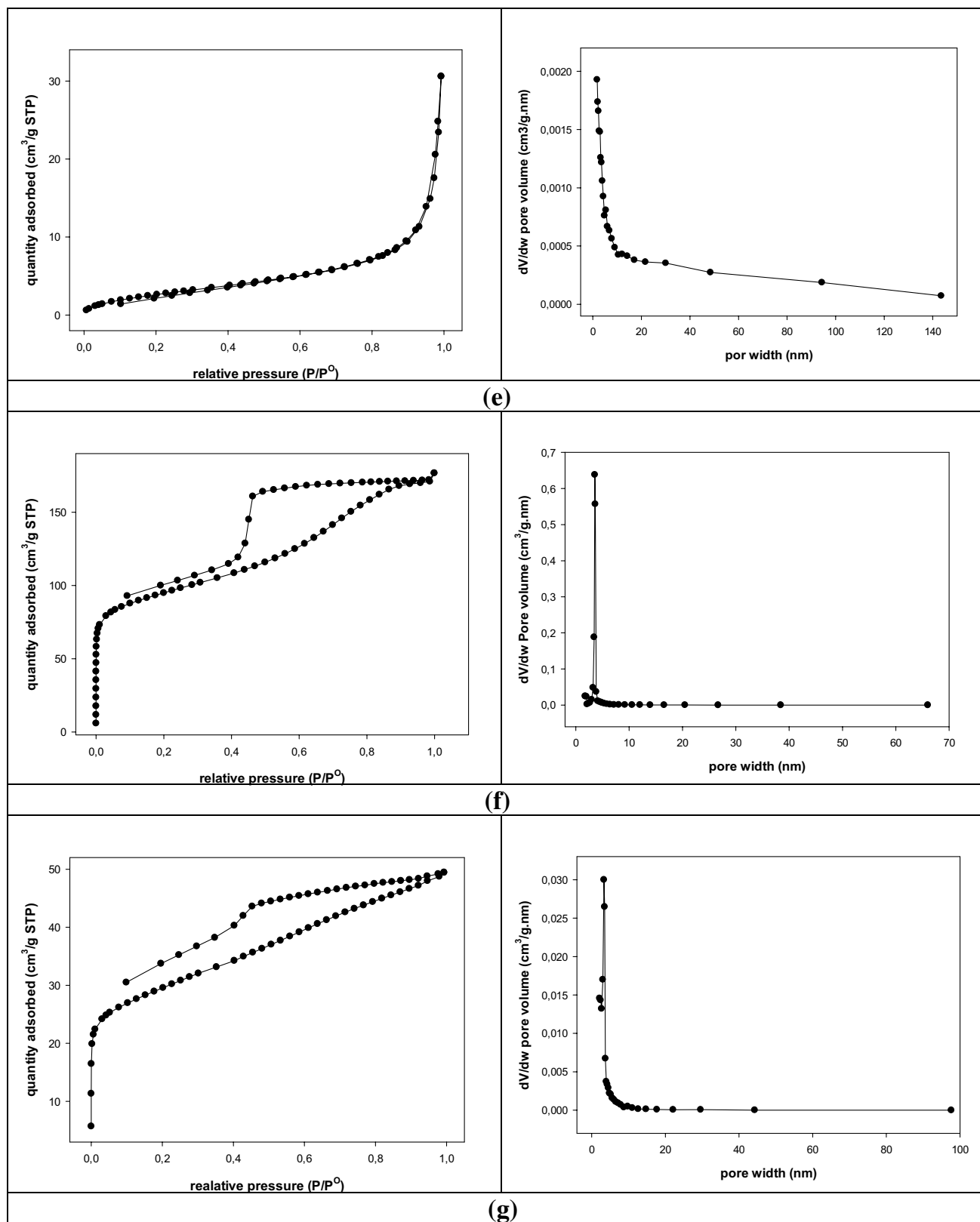
(e)

(f)
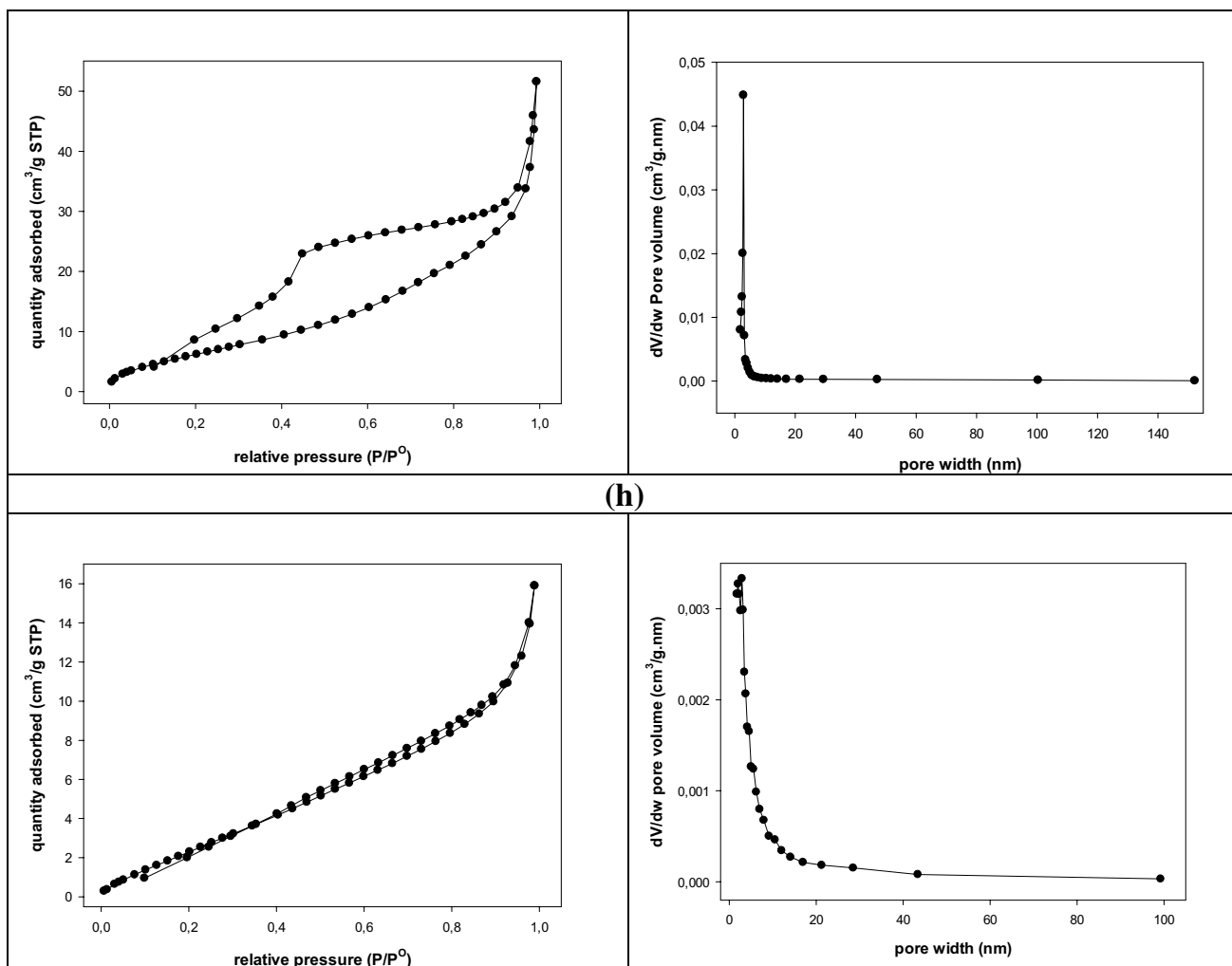

(g)

**Fig. 4** (continued)

(h)

Fig. 4 (continued)

Table 3 Structural properties of synthesized materials

Sample	BET surface area (m^2 g^{-1})	Average pore diameter (nm)	Langmuir surface area (m^2 g^{-1})	t-Plot external surface area (m^2 g^{-1})	Average particle size (nm)	BJH surface area (m^2 g^{-1})	D-H surface area (m^{2}g^{-1})	BJH pore volume (cm^3 g^{-1})	D-H pore volume (cm^3 g^{-1})
CXA1	83.9	3.471	197.676	65.282	71.532	52.977	51.434	0.054	0.053
CX1	52.7	3.537	132.839	46.263	113.791	33.257	32.302	0.035	0.034
CXA1/PPy	4.6	13.461	281.678	6.389	1315.650	7.757	8.588	0.040	0.043
CX1/PPy	10.9	7.621	97.464	15.114	550.603	11.313	13.772	0.046	0.049
CXA2	312.3	3.363	705.156	159.386	19.213	175.647	173.395	0.182	0.179
CX2	98.9	3.013	210.247	59.619	60.650	48.808	47.491	0.046	0.030
CXA2/PPy	26.0	7.782	298.420	37.618	230.570	40.777	60.736	0.075	0.091
CX2/PPy	13.1	5.616	154.430	21.467	459.334	14.690	18.062	0.024	0.028

xerogel structures exhibited thermal stability up to about 450 °C and negligible mass loss was observed (5%). Mass loss was observed more rapidly and linearly in the temperature range of 450–1190 °C. It was observed that the thermal as the surface area increases. The material with the highest thermal durability is CX1 (52.7 m^{2}g^{-1}) and the lowest one is CXA2 (312.3 m^2 g^{-1}). CX1 and CXA2 xerogels were completely combusted at 1190 °C and 875 °C, respectively.

Fig. 5 SEM images of **a** CX1, **b** CXA1, **c** CX1/PPy, **d** CXA1/PPy, **e** CX2, **f** CXA2, **g** CX2/PPy, **h** CXA2/PPy
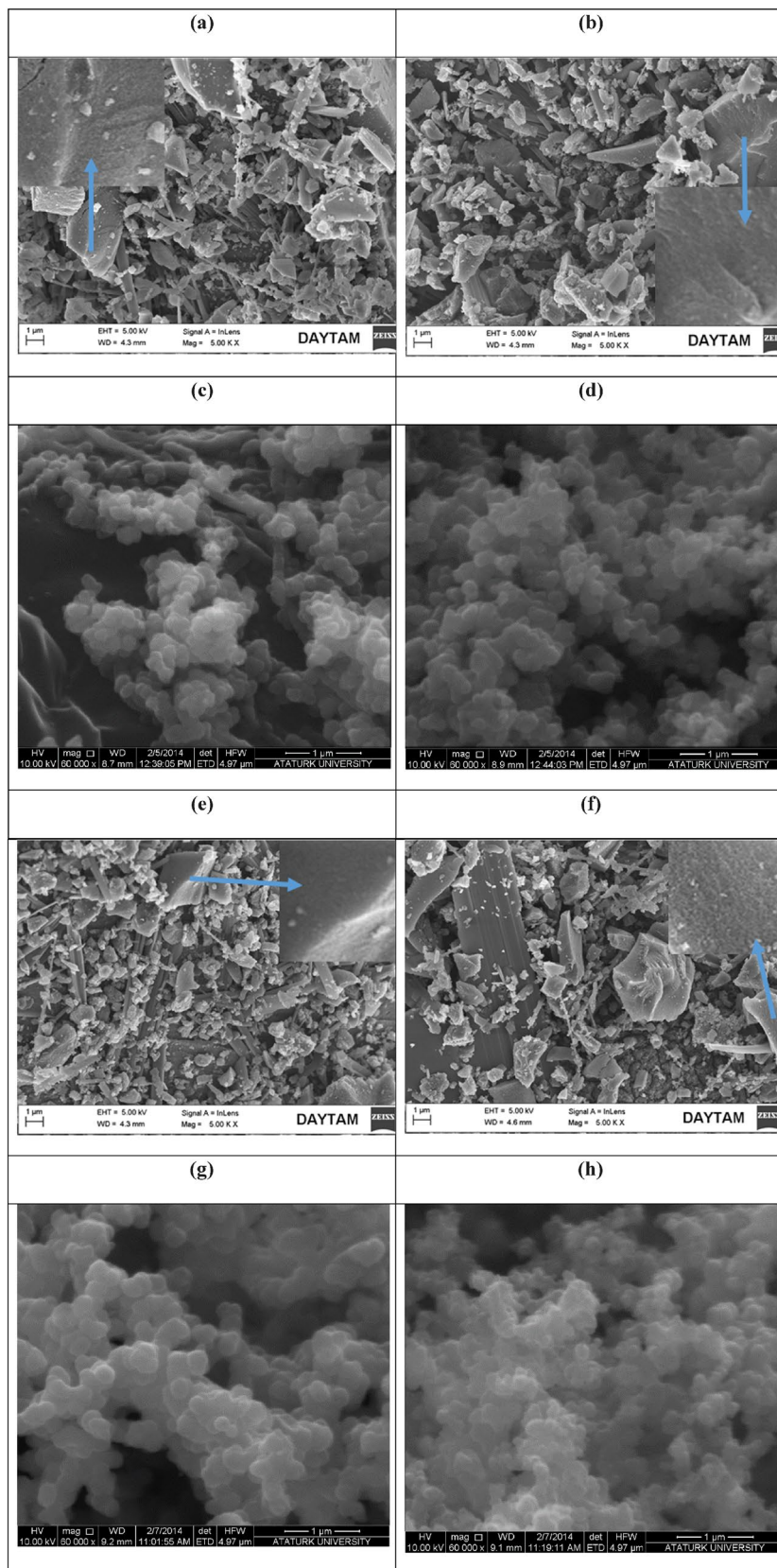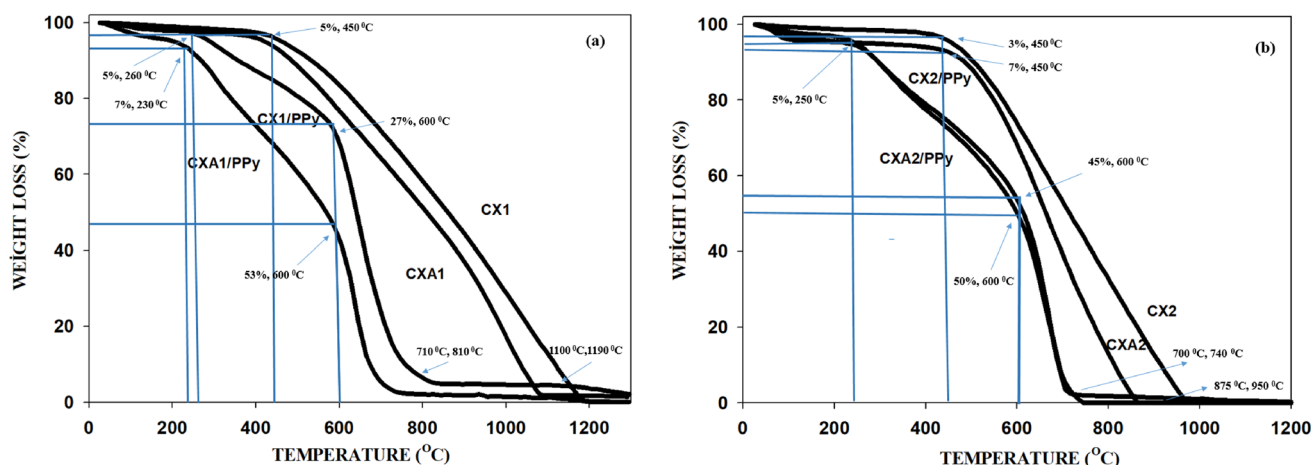
Fig. 6 TGA analysis of **a** CXA1, CX1 and their polypyrrole composites, **b** CXA2, CX2 and their polypyrrole composites

The situation is different for PPy/carbon xerogel composites. PPy is a material that degrades at lower temperatures (at an average temperature of 450 °C) than carbonaceous materials [54]. Therefore, the addition of PPy to carbon xerogel structures caused a decrease in thermal stability. In general, a negligible mass loss to PPy composites 230–260 °C (5%) was observed due to removal of the oxygen-containing functional groups. Decomposition of the polymer took place in the 230–600 °C temperature range. The amount of PPy in the composites may differ between each other due to the different pore size distributions of carbon xerogels as shown in Fig. 4 and the BJH pore volume values given in Table 3. Pore size distributions and open pores affect the coating rate of PPy on xerogel surfaces. The increase in mesopore density increased the amount of coating PPy on the xerogel surface. This is supported by the SEM images. At 600 °C, PPy is completely consumed in composites. The mass loss ratios at 600 °C of CX1/PPy, CXA1/PPy, CX2/PPy and CXA2/PPy composites were 27%, 53%, 45% and 50%, respectively.

CX, CXA and their PPy composites were electrochemically characterized and capacitive properties were investigated. Cyclic voltammograms (CV) of carbon xerogels and their polypyrrole composites in different potential ranges (0.3, 0.5, 0.7 and 0.9 V upper potential, 50 mVs^{-1} scan rate and H_2SO_4 environment) are given in Fig. 7 as before and after 1000 cycles. Looking at the CV curves of carbon xerogels before 1000 cycles, it can be seen that it exhibits a typical rectangular shape indicating ideal electrical double layer capacitive behavior. CXA2 xerogel exhibited the most distinctive rectangular structure due to its enhanced surface area properties (312.3 m^2 g^{-1}). In contrast, when we look at CV curves of carbon xerogels after 1000 cycles, it shows the presence of hydroquinone molecules (hydroquinone $\leftrightarrow$ quinone $+ 2H^+ + 2e^-$) adsorbed on the xerogel surface due to the carbon corrosion of the peak in the range of 0.5–0.7 V.

This shows the coexistence of both electrical double layer capacitance and pseudocapacitance. With the addition of polypyrrole, CV curves have a more rectangular shape compared to xerogels. This indicates that the pseudo-capacitive effect is more dominant in composite xerogel structures. This shows that the counter ions can easily penetrate and reach the inner surface of the polymer matrix and that the polypyrrole occurs in redox reactions other than ion migration due to its structure. These reactions occur with the presence of electrochemically active regions in the structure due to the N (nitrogen) source of polypyrrole [55]. Therefore, the supercapacitor combines two types of energy storage at the same time. One is pure electrostatic attraction (non-faradic reactions) between the ions and the charged electrode surface, and the other is pseudocapacity (faradayic reactions) as a result of redox reactions caused by PPy [56]. Polypyrrole may form channels between the mesopores that allow electrolyte access. These channels may become clogged if they form a thicker film on the carbon xerogel surface of the polypyrrole. In this case, there may also be reductions in the specific capacitance of the composite structures [57]. It was observed that the higher the potential upper limit, the higher the specific capacitance. This shows that ion diffusion is higher with the decrease in resistance due to the potential increase in the electrolyte in the network structure of carbon xerogel.

Figure 8 shows the CV curves of the synthesized materials at various scan rates from 5 to 500 mVs^{-1}. Anodic current peak and cathodic current peak are very weak at low scanning speeds. The peak potential difference increased with increasing scanning speed. It is observed that the peaks of composites are more prominent after 1000 cycles. In carbon xerogels, the specific capacitance is observed to be diffusion controlled. In PPy composites, it is observed that internal resistance is more effective with increasing scanning
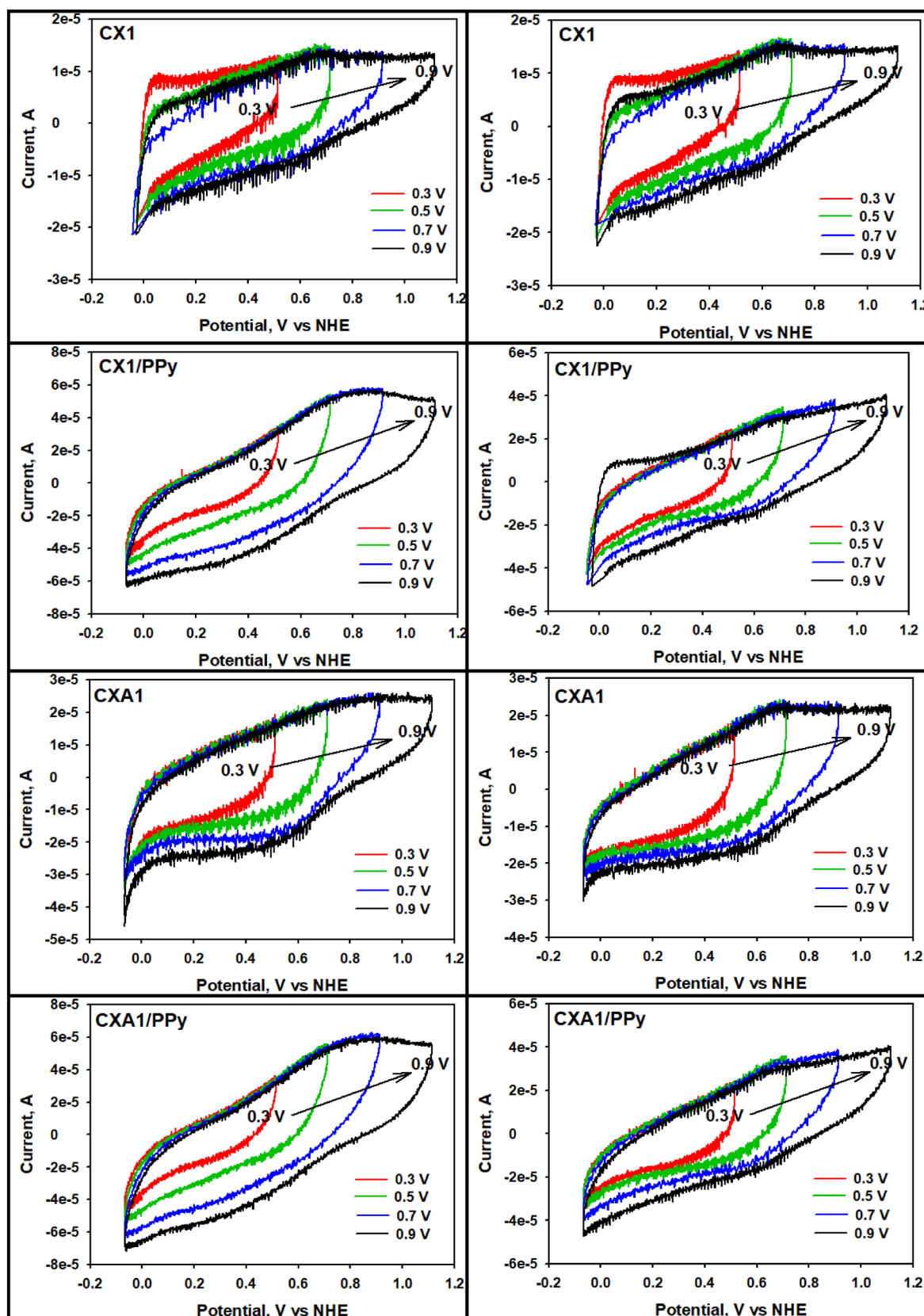
Fig. 7 The cycling voltammograms of the synthesized materials at the different potential range (at a potential limit of 0.3, 0.5, 0.7 and 0.9 V, the scan rate of 50 mV s^{-1} and in the 1M H$_2$SO$_4$ medium)
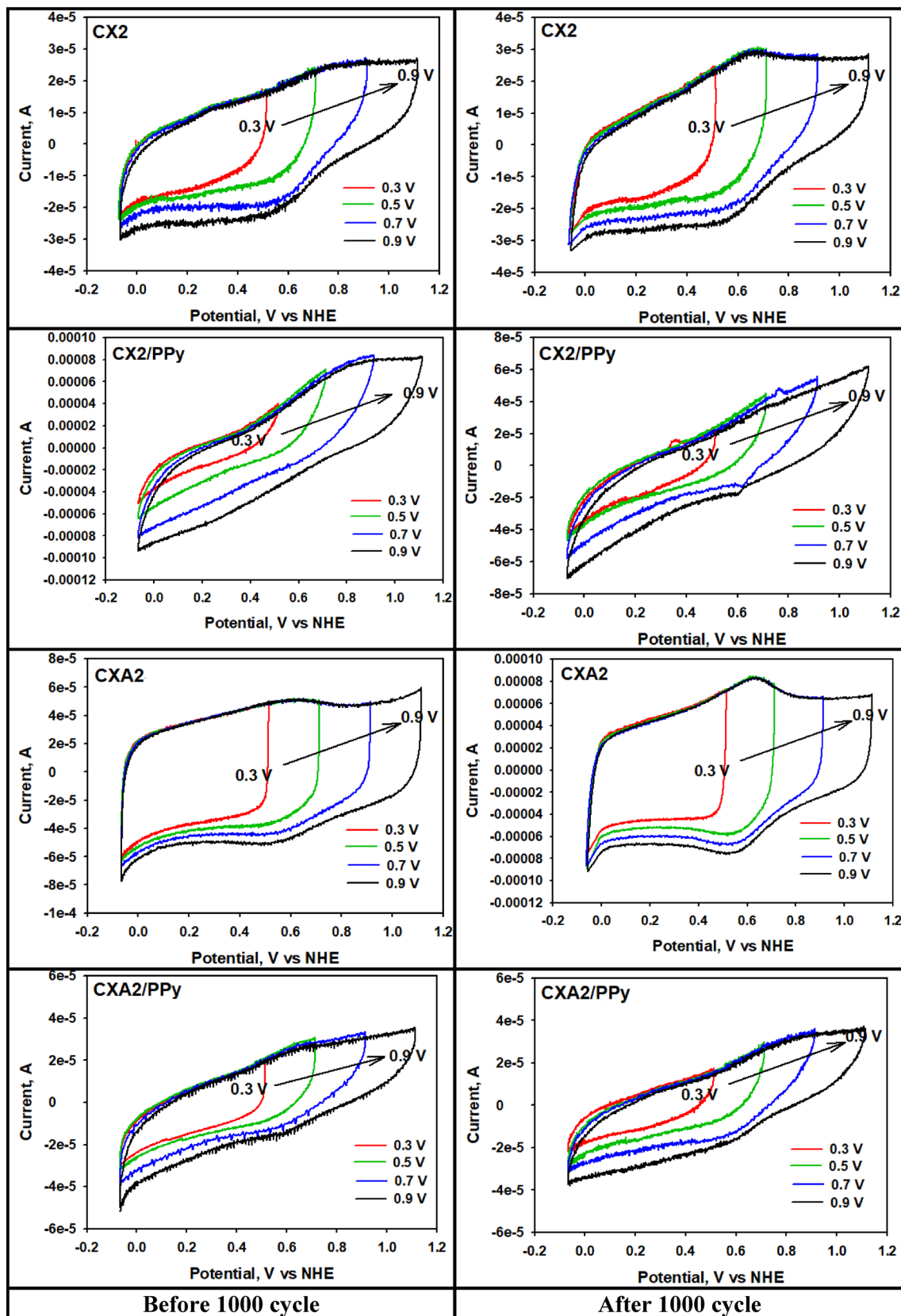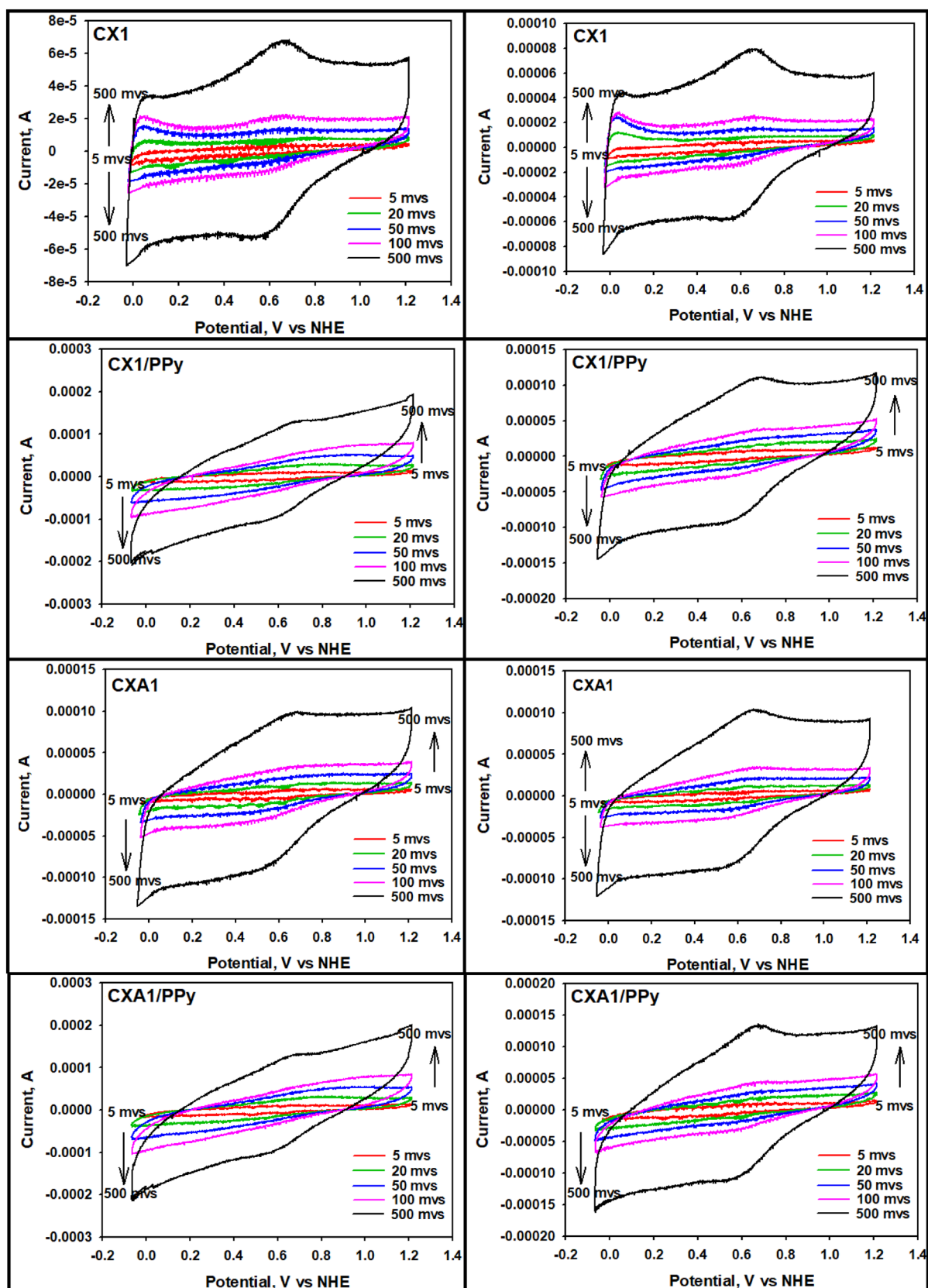
Fig. 7 (continued)

Fig. 8 The cycling voltammograms of the synthesized materials at the different scan rates (5, 20, 50, 100, 500 mV s^{-1} and 1M H$_2$SO$_4$ medium)

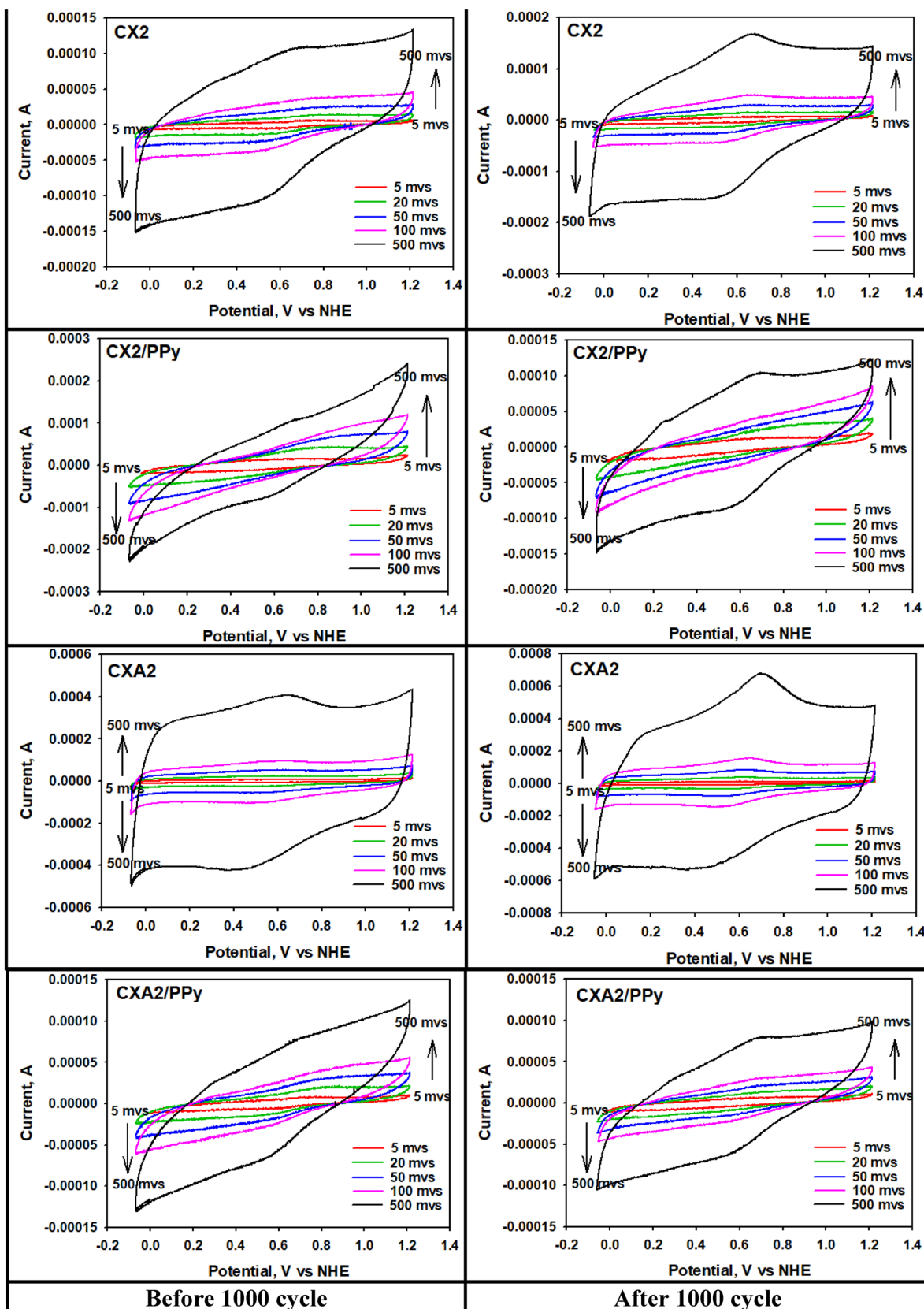**Before 1000 cycle** | **After 1000 cycle**

Fig. 8 (continued)

speed. This may be because the concentration of ions at the electrode/electrolyte interface increases rapidly, and consequently the diffusion rate is not sufficient for electrochemical reactions [22].

Specific capacitance values of materials synthesized using cyclic voltammograms at different scanning speeds (5, 20, 50, 100, 500 mVs^{-1}) and before–after 1000 cycles were calculated from the CV results and are shown in Table 4. Very small increases in specific capacitance of carbon xerogels occurred after 1000 cycles. The reason for this is the carbon corrosion that we explained in Fig. 7 [58]. It is seen that the three-dimensional structure of carbon xerogels and the polypyrrole conductive polymer interact very well (with the presence of electrochemical active areas as N source). As a result of this interaction, a composite structure that combines the superior properties of carbon xerogel and polypyrrole has been obtained. The conductive polymer matrix evenly covered the surface of the carbon xerogel, allowing rapid entry and exit of the ion, resulting in an increase in specific capacitance overall.

The specific capacitance values of carbon xerogel and polypyrrole composites with an R/C ratio of 100 increased with the effect of solvent exchange process with acetone. This situation showed that the solvent exchange process with acetone positively affect the BET surface areas and pore size distributions. SEM images also support this situation. Solvent exchange with acetone provided a more intense and homogeneous spread of the PPy film layer on the xerogel surface. In materials with an R/C ratio of 100, the highest specific capacitance belongs to CXA1/PPy material with 440 Fg^{-1} at 5 mVs^{-1} and 1000 cycles.

Increasing the R/C ratio from 100 to 200 positively affects the specific capacitances of materials other than CXA2/PPy. The specific capacitance of carbon xerogel subjected to solvent exchange treatment with acetone is twice that of carbon xerogel without solvent exchange. This is explained by the fact that the BET surface areas of the xerogels with

an R/C ratio of 200 significantly increased with the effect of solvent exchange with acetone (CX2, 98.8 m^2 g^{-1}, 222 Fg^{-1}; CXA2, 312.3 m^2 g^{-1}, 442 Fg^{-1}). Among PPy composites, the highest specific capacitance value belongs to CX2/PPy composite. The specific capacitance of CX2/PPy composite reached to 599 Fg^{-1} at 5 mVs^{-1}. Only the specific capacitance value of the CXA2/PPy composite unexpectedly decreased. This result is related to the film thickness of PPy coated on the surface of the CXA2 xerogel. Low or high PPy film thickness affects the capacitance negatively [36]. Apart from this, a decrease in the specific capacitance of PPy composite structures was measured at the end of 1000 cycles. This shows that composites have poor mechanical strength.

There are some studies on carbonaceous materials and conductive polymers forming composites. Chen et al. increased the specific capacitance from 92 to 180 Fg^{-1} by adding polyaniline to pure carbon [59]. You et al. increased the specific capacitance to 180 Fg^{-1} by adding pyrrole as a nitrogen source of graphene-carbon nanotube composite [55]. Lee et al., combining carbon nano spheres with melamine as the N source, reached 191.91 Fg^{-1} specific capacitance [60]. Samancı et al. increased the specific capacitance from 147 to 231 Fg^{-1} by adding polypyrrole to carbon aerogel structures [37].

Specific capacitance retention percentages of PPy composites (CXA1/PPy, CX1/PPy, CXA2/PPy and CX2/PPy) at the end of 1000 cycles are shown in Table 5. Capacitance retention values were realized at the highest 500 mVs^{-1} and the lowest at 5 mVs^{-1}. The material with the highest capacitance retention percentage at 5 mVs^{-1} is CXA2/PPy with 95.94%. The material with the lowest percentage of capacitance retention at 5 mVs^{-1} is for CX1/PPy material as 75.78%. The capacitance retention percentage resulted in inversely proportional to the thickness of the PPy film coated in the composite. This situation can be explained by physicochemical analysis (BET, SEM and TGA). To obtain a high and stable specific capacitance in

Table 4 The specific capacitance values of the synthesized materials at different scan rates for before and after 1000 cycles

Sample	Specific capacitance (Fg^{-1})									
	Before 1000 cycles					After 1000 cycles				
	scan rates (mVs^{-1})					scan rates (mVs^{-1})				
	5	20	50	100	500	5	20	50	100	500
CX1	137	89	65	50	31	179	108	75	57	35
CX1/PPy	417	270	183	129	60	316	177	113	84	50
CXA1	203	130	94	73	43	207	146	101	79	55
CXA1/PPy	440	286	188	129	61	366	199	128	97	59
CX2	222	157	119	95	59	265	174	136	115	80
CX2/PPy	599	360	214	131	47	481	257	143	95	47
CXA2	442	378	335	304	243	577	477	426	392	300
CXA2/PPy	271	175	115	80	37	260	142	91	67	35

Table 5 Specific capacitance retention percentages of materials synthesized at different scanning rates at the end of 1000 cycles

Sample	Capacitance retention (%)				
	scan rates (mVs^{-1})				
	5	20	50	100	500
CX1/PPy	75.78	65.55	61.75	65.12	83.33
CXA1/PPy	83.18	69.58	68.09	75.19	96.72
CX2/PPy	80.30	71.38	66.82	72.52	100
CXA2/PPy	95.94	81.14	79.13	83.75	94.59

composite xerogels, the specific surface area, pore characteristics and film thickness (film microstructure) of the electroactive regions should be better controlled. The change in the microstructure of the polypyrrole film affects the penetration of the electrolyte into the pores and the ion mobility within the conductive polymer [57]. The thickness of the PPy film should be at optimum values. Thin film causes easy deformation of PPy. Thick film, on the other hand, cuts the connection between PPy and carbon structure and causes an increase in internal resistance. In these two cases, the specific capacitance decreases.

There are many studies in the literature on polypyrrole composites made with different carbonaceous materials. Table 6 summarizes some of the studies on this subject. It was observed that PPy composites with carbon materials generally have 80% and above capacitance retention for an average of 1000 cycles. Studies have shown that in long-term charging and discharging conditions, volumetric changes in the structure of PPy and consequently, decreases in electrical conductivity as a result of deterioration in the bond structure of PPy. The carbon xerogel and their PPy composites synthesized in this study show very good capacitance values compared to the studies in the literature. At the end of 1000 cycles, an average value of capacitance retention was measured.

Electrochemical impedance spectroscopy (EIS) is a widely used method of analysis to investigate the redox processes of electrode materials (about the capacitive and resistive behavior of the samples studied) and to evaluate their electronic and ionic conductivity. The power output capacity of the supercapacitor depends not only on the ionic mass transport speeds, but also on the series resistance (R) (depending on the frequency, that is to say, the rate of the process). R contains both electronic and ionic resistance [19, 67]. Resistant behavior of the synthesized materials was determined by EIS experiments by applying 0.4, 0.65 and 0.9 V potentials. Nyquist plots of CXA1, CX, CX2, CXA2 and polypyrrole composites before and after aging are shown in Figs. 9, 10. As can be seen from Figs. 9, 10, there is not much change in the resistances after aging. There is not much change in the internal resistances of CX1A, CX, CX2, CXA2 and polypyrrole composites according to the change in the potentials. It was observed that carbon xerogel materials responds to an impedance close to the ideal capacitor and it deviates from the ideal state with the addition of polypyrrole and its internal resistance is increased [67]. Different tendencies were observed for different materials before and after aging. It was observed that both the structural properties of the material and the applied potential affect the internal resistances. Since the pore size distribution of xerogels applied with solvent change is better controlled, they have an improved surface area. The most important parameter affecting performance in supercapacitors is the specific surface area of the material. In xerogels with suitable pore size, the resistance becomes even less, since the ion entry and exit into the pore is easier. It is seen that due to the increase in the potential ratio, both the increase of the ion input–output and the increase in the redox reactions into the composite structure, it is seen that there is a deterioration in the polymer

Table 6 Some literature studies on the composites of polypyrrole made with carbonaceous materials

| Sample	Specific capacitance (Fg^{-1})	Electrolyte	Scan rates (mVs^{-1})	Cycles	Capacitance retention (%)	Ref.
3DOM CNT/PPy	472	1-M KCl	5	1000	89.9	[61]
PPy/F-MWNTs	240	2-M KCl	10	1000	93.49	[62]
PPY–MWCNT	310	0.5-M Na$_2$SO$_4$	2	1000	85	[63]
CNF@G/PPy	386	0.5-M Na$_2$SO$_4$	2	1000	84	[64]
PPy/CA	433	6-M KOH	1	500	–	[43]
GO/CNF/PPy films	144.6	1-M H$_2$SO$_4$	10	5000	89	[65]
PPy/C	~395	0.5-M Na$_2$SO$_4$	100	~500	100	[66]
RGO/PPy	424	1-M H$_2$SO$_4$	100	–	–	[56]
PPy/CA1	231	1-M H$_2$SO$_4$	50	1000	51	[37]
CX2/PPy	599	1-M H$_2$SO$_4$	5	1000	80.30	Our work
CXA1/PPy	440	1-M H$_2$SO$_4$	5	1000	83.18	Our work
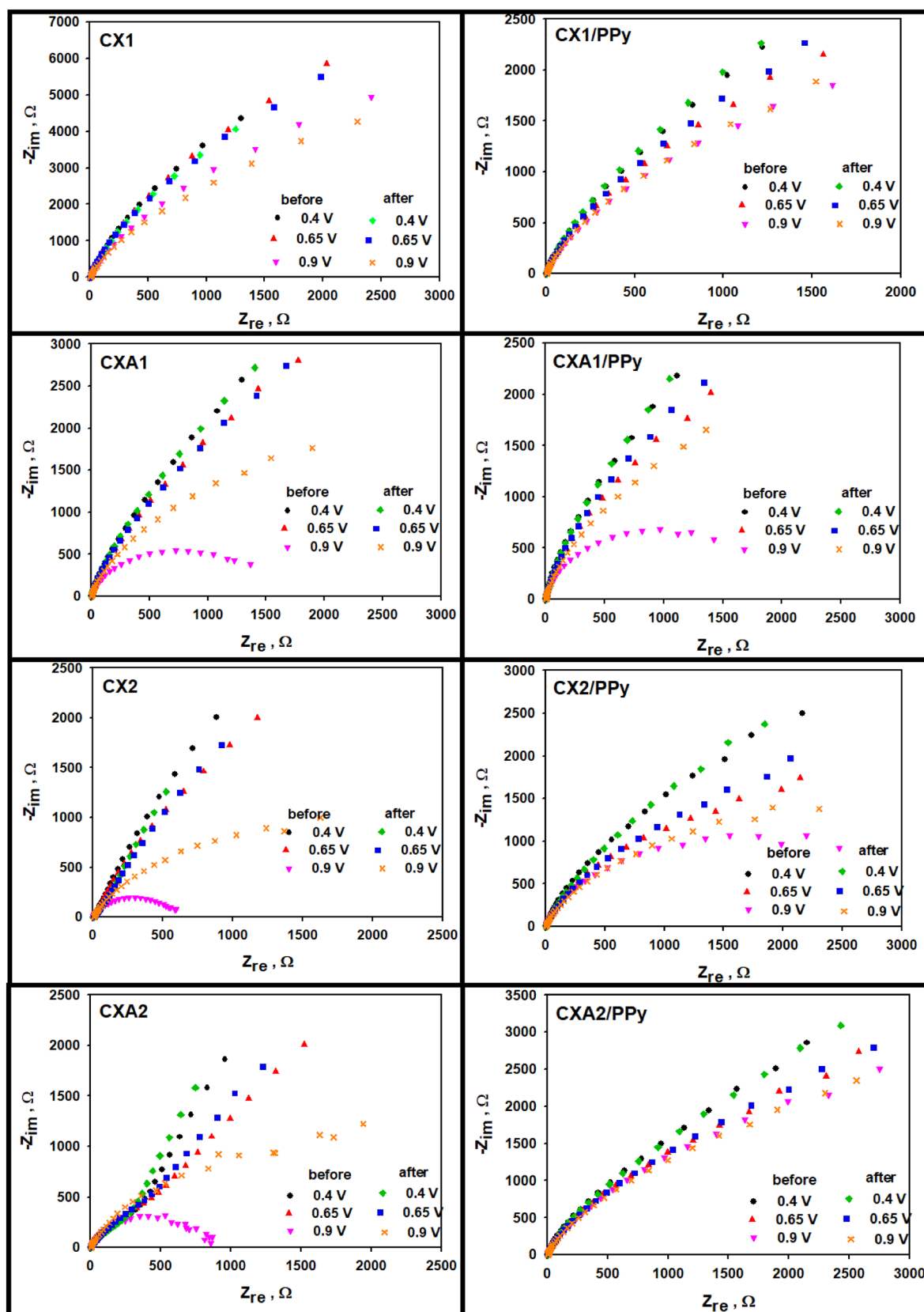
Fig. 9 Nyquist plots obtained at different potentials before and after aging of CX1, CXA1, CX2, CXA2 and composites with polypyrrole (at 0.4, 0.65 and 0.9 V potentials in 1M H_2SO_4 solution)
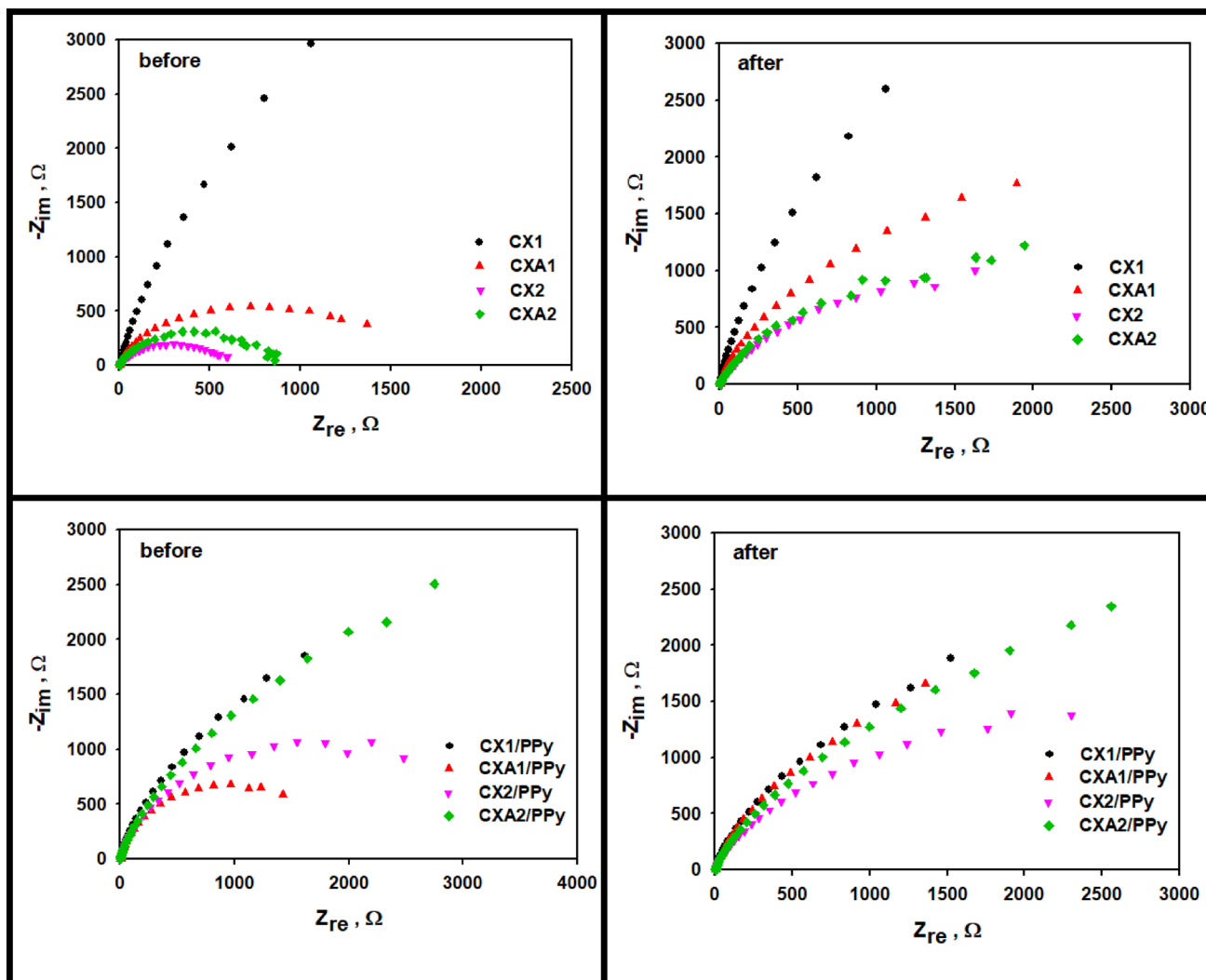
Fig. 10 Nyquist plots obtained at 0.9 V before and after aging of CX1, CXA1, CX2, CXA2 and their composites with polypyrrole

matrix. To obtain a high and stable specific capacitance in composites of carbon xerogels, the specific surface area, pore characteristics and film thickness (film microstructure) of the electroactive regions should be better controlled. The change in the microstructure of the polypyrrole film affects the penetration of the electrolyte into the pores and the ion mobility within the conductive polymer.

5 Conclusions

In recent years, carbonaceous materials are widely used, especially in energy storage systems such as supercapacitors. In addition, researchers are synthesizing composites with conductive polymers or transition metal oxides to improve the performance of carbonaceous materials. In this study, carbon xerogel structures, which are three-dimensional

carbon materials, and their composites with conductive polymer polypyrrole were synthesized. Thus, the performance of carbon xerogel and the mechanical strength of PPy were tried to be increased. Carbon xerogels were prepared using the sol–gel technique by drying under ambient conditions. With this drying technique, it is carried out by drying under ambient conditions that are easy, low cost and safe. Polypyrrole/carbon xerogel composites were synthesized using chemical polymerization technique. As parameters in synthesized materials, R/C ratios, solvent exchange or not, and the effects of doping of polypyrrole on the structure and specific capacitance were investigated. In PPy composite synthesis, it has been observed that PPy film thickness is effective in the specific capacitance of the electrode. Among the synthesized materials, the highest specific capacitance values belong to polypyrrole/carbon xerogel composites. As a result of the analysis and calculations, it was found that the

highest specific capacitance belongs to CX2/PPy composite with 599 Fg^{-1} at 5 mVs^{-1}. CX2/PPy composite has been found to have a capacitance retention rate of 80.30% at the end of 1000 cycles.

References

1. Kim BK, Sy S, Yu A, Zhang J (2015) Electrochemical supercapacitors for energy storage and conversion. In: Yan J (ed) Handbook of clean energy systems. Wiley, Chichester
2. Saravanakumara B, Muralidharanb G, Vadivel S, Maruthamani D, Kumaravel M (2018) Theory, fundamentals and application of supercapacitors. In: Asiri AM, Inamuddin, Ahmer MF (eds) Electrochemical capacitors: theory, materials and applications . Materials Research Forum LLC, Millersville
3. Wu Z, Zhu Y, Ji X, Banks CE (2016) Transition metal oxides as supercapacitor materials. In: Ozoemena KI, Shaowei C (eds) Nanomaterials in Advanced Batteries and Supercapacitors. Springer, Cham
4. Kandalkar S, Dhawale D, Kim C-K, Lokhande C (2010) Chemical synthesis of cobalt oxide thin film electrode for supercapacitor application. Synth Met 160(11–12):1299–1302. https://doi.org/10.1016/j.synthmet.2010.04.003
5. Bryan AM, Santino LM, Lu Y, Acharya S, D'Arcy JM (2016) Conducting polymers for pseudocapacitive energy storage. Chem Mater 28(17):5989–5998. https://doi.org/10.1021/acs.chemmater.6b01762
6. Conway B (1999) Similarities and differences between supercapacitors and batteries for storing electrical energy. In: Conway B (ed) Electrochemical supercapacitors. Springer, Boston
7. Mombeshora ET, Nyamori VO (2015) A review on the use of carbon nanostructured materials in electrochemical capacitors. Int J Energy Res 39(15):1955–1980. https://doi.org/10.1002/er.3423
8. Ramos-Fernández G, Canal-Rodríguez M, Arenillas A, Menéndez JA, Rodríguez-Pastor I, Martin-Gullon I (2018) Determinant influence of the electrical conductivity versus surface area on the performance of graphene oxide-doped carbon xerogel supercapacitors. Carbon 126:456–463. https://doi.org/10.1016/j.carbon.2017.10.025
9. Zhang LL, Zhao S, Tian XN, Zhao X (2010) Layered graphene oxide nanostructures with sandwiched conducting polymers as supercapacitor electrodes. Langmuir 26(22):17624–17628. https://doi.org/10.1021/la103413s
10. Fan T, Tong S, Zeng W, Niu Q, Liu Y, Kao C-Y, Liu J, Huang W, Min Y, Epstein AJ (2015) Self-assembling sulfonated graphene/polyaniline nanocomposite paper for high performance supercapacitor. Synth Met 199:79–86. https://doi.org/10.1016/j.synthmet.2014.11.017
11. Lin YH, Wei TY, Chien HC, Lu SY (2011) Manganese oxide/carbon aerogel composite: an outstanding supercapacitor electrode material. Adv Energy Mater 1(5):901–907. https://doi.org/10.1002/aenm.201100256
12. Nguyen TT, Shim J-J (2015) Rapid one-step synthesis and electrochemical properties of graphene/carbon nanotubes/MnO2 composites. Synth Met 199:276–279. https://doi.org/10.1016/j.synthmet.2014.12.006
13. Jo S, Park YH, Ha S-G, Kim SM, Song C, Park SY, In I (2015) Simple noncovalent hybridization of polyaniline with graphene and its application for pseudocapacitor. Synth Met 209:60–67. https://doi.org/10.1016/j.synthmet.2015.06.004
14. Sardar A, Gupta P (2018) Polypyrrole based nanocomposites for supercapacitor applications: A review. In: AIP Conference Proceedings. vol 1. AIP Publishing LLC, 030020; https://doi.org/10.1063/1.5032355
15. Patil B, Jagadale A, Lokhande C (2012) Synthesis of polythiophene thin films by simple successive ionic layer adsorption and reaction (SILAR) method for supercapacitor application. Synth Met 162(15–16):1400–1405. https://doi.org/10.1016/j.synthmet.2012.05.023
16. Zhao Z, Richardson GF, Meng Q, Zhu S, Kuan H-C, Ma J (2015) PEDOT-based composites as electrode materials for supercapacitors. Nanotechnology 27(4):042001. https://doi.org/10.1088/0957-4484/27/4/042001
17. Groenendaal L, Jonas F, Freitag D, Pielartzik H, Reynolds JR (2000) Poly (3, 4-ethylenedioxythiophene) and its derivatives: past, present, and future. Adv Mater 12(7):481–494. https://doi.org/10.1002/(SICI)1521-4095(200004)12
18. Konwer S, Boruah R, Dolui SK (2011) Studies on conducting polypyrrole/graphene oxide composites as supercapacitor electrode. J Electron Mater 40(11):2248. https://doi.org/10.1007/s11664-011-1749-z
19. Wang J, Xu Y, Chen X, Sun X (2007) Capacitance properties of single wall carbon nanotube/polypyrrole composite films. Compos Sci Technol 67(14):2981–2985. https://doi.org/10.1016/j.compscitech.2007.05.015
20. An H, Wang Y, Wang X, Li N, Zheng L (2010) The preparation of PANI/CA composite electrode material for supercapacitors and its electrochemical performance. J Solid State Electrochem 14(4):651–657. https://doi.org/10.1007/s10008-009-0835-0
21. Alvi F, Ram MK, Basnayaka P, Stefanakos E, Goswami Y, Hoff A, Kumar A (2011) Electrochemical supercapacitors based on graphene-conducting polythiophenes nanocomposite. ECS Trans 35(34):167. https://doi.org/10.1149/1.3654215
22. Mitchell E, Candler J, De Souza F, Gupta R, Gupta BK, Dong L (2015) High performance supercapacitor based on multilayer of polyaniline and graphene oxide. Synth Met 199:214–218. https://doi.org/10.1016/j.synthmet.2014.11.028
23. Tang W, Peng L, Yuan C, Wang J, Mo S, Zhao C, Yu Y, Min Y, Epstein AJ (2015) Facile synthesis of 3D reduced graphene oxide and its polyaniline composite for super capacitor application. Synth Met 202:140–146. https://doi.org/10.1016/j.synthmet.2015.01.031
24. Li F, Xie L, Sun G, Kong Q, Su F, Cao Y, Wei J, Ahmad A, Guo X, Chen C-M (2019) Resorcinol-formaldehyde based carbon aerogel: preparation, structure and applications in energy storage devices. Microporous Mesoporous Mater 279:293–315. https://doi.org/10.1016/j.micromeso.2018.12.007
25. Chavhan M, Ganguly S (2017) Carbon cryogel from resorcinol formaldehyde: tuning of processing steps and activation for use in supercapacitor. Mater Technol 32(12):744–754. https://doi.org/10.1080/10667857.2017.1351145
26. Job N, Théry A, Pirard R, Marien J, Kocon L, Rouzaud J-N, Béguin F, Pirard J-P (2005) Carbon aerogels, cryogels and xerogels: influence of the drying method on the textural properties of porous carbon materials. Carbon 43(12):2481–2494. https://doi.org/10.1016/j.carbon.2005.04.031
27. Li J, Wang X, Wang Y, Huang Q, Dai C, Gamboa S, Sebastian P (2008) Structure and electrochemical properties of carbon aerogels synthesized at ambient temperatures as supercapacitors. J Non Cryst Solids 354(1):19–24. https://doi.org/10.1016/j.jnoncrysol.2007.07.024
28. Wang X, Liu L, Wang X, Bai L, Wu H, Zhang X, Yi L, Chen Q (2011) Preparation and performances of carbon aerogel microspheres for the application of supercapacitor. J Solid

State Electrochem 15(4):643–648. https://doi.org/10.1007/s10008-010-1142-5

29. Saliger R, Bock V, Petricevic R, Tillotson T, Geis S, Fricke J (1997) Carbon aerogels from dilute catalysis of resorcinol with formaldehyde. J Non-Cryst Solids 221(2–3):144–150. https://doi.org/10.1016/S0022-3093(97)00411-0

30. Li J, Wang X, Huang Q, Gamboa S, Sebastian P (2006) Studies on preparation and performances of carbon aerogel electrodes for the application of supercapacitor. J Power Sources 158(1):784–788. https://doi.org/10.1016/j.jpowsour.2005.09.045

31. Lee YJ, Jung JC, Yi J, Baeck S-H, Yoon JR, Song IK (2010) Preparation of carbon aerogel in ambient conditions for electrical double-layer capacitor. Curr Appl Phys 10(2):682–686. https://doi.org/10.1016/j.cap.2009.08.017

32. Pekala R, Schaefer D (1993) Structure of organic aerogels. 1. Morphology and scaling. Macromolecules 26(20):5487–5493. https://doi.org/10.1021/ma00072a029

33. Job N, Pirard R, Marien J, Pirard J-P (2004) Porous carbon xerogels with texture tailored by pH control during sol–gel process. Carbon 42(3):619–628. https://doi.org/10.1016/j.carbon.2003.12.072

34. Barım ŞB, Bayrakçeken A, Bozbağ SE, Zhang L, Kızılel R, Aindow M, Erkey C (2017) Control of average particle size of carbon aerogel supported platinum nanoparticles by supercritical deposition. Microporous Mesoporous Mater 245:94–103. https://doi.org/10.1016/j.micromeso.2017.01.037

35. Kim S-J, Hwang S, Hyun S (2005) Preparation of carbon aerogel electrodes for supercapacitor and their electrochemical characteristics. J Mater Sci 40(3):725–731. https://doi.org/10.1007/s10853-005-6313-x

36. Wang J, Li X, Du X, Wang J, Ma H, Jing X (2017) Polypyrrole composites with carbon materials for supercapacitors. Chem Pap 71(2):293–316. https://doi.org/10.1007/s11696-016-0048-9

37. Samancı M, Daş E, Bayrakçeken Yurtcan A (2021) Carbon aerogel and their polypyrrole composites used as capacitive materials. Int J Energy Res 45(2):1729–1747. https://doi.org/10.1002/er.5841

38. Zhu M, Weber C, Yang Y, Konuma M, Starke U, Kern K, Bittner A (2008) Chemical and electrochemical ageing of carbon materials used in supercapacitor electrodes. Carbon 46(14):1829–1840. https://doi.org/10.1016/j.carbon.2008.07.025

39. Anneser K, Reichstein J, Braxmeier S, Reichenauer G (2018) Carbon xerogel based electric double layer capacitors with polymer gel electrolytes–improving the performance by adjusting the type of electrolyte and its processing. Electrochim Acta 278:196–203. https://doi.org/10.1016/j.electacta.2018.05.046

40. Awadallah-F A, Al-Muhtaseb SA (2019) Influence of chitosan addition on resorcinol-formaldehyde xerogel structure. Appl Sci 9(21):4582. https://doi.org/10.3390/app9214582

41. Al-Muhtaseb SA, Ritter JA (2003) Preparation and properties of resorcinol–formaldehyde organic and carbon gels. Adv Mater 15(2):101–114. https://doi.org/10.1002/adma.200390020

42. Jun S, Weina H, Yijie M, Yangling O, Guangming W, Bin Z, Zhihua Z, Xingyuan N, Xixian N, Guoqing W (2008) Nanostructure control of carbon aerogels and the application in lithium ion cells. In: 2nd IEEE International Nanoelectronics Conference, pp 74–77. https://doi.org/10.1109/INEC.2008.4585440

43. An H, Wang Y, Wang X, Zheng L, Wang X, Yi L, Bai L, Zhang X (2010) Polypyrrole/carbon aerogel composite materials for supercapacitor. J Power Sources 195(19):6964–6969. https://doi.org/10.1016/j.jpowsour.2010.04.074

44. Li W-C, Lu A-H, Guo S-C (2001) Characterization of the microstructures of organic and carbon aerogels based upon mixed cresol–formaldehyde. Carbon 39(13):1989–1994. https://doi.org/10.1016/S0008-6223(01)00029-X

45. Bakos LP, Mensah J, László K, Igricz T, Szilágyi IM (2018) Preparation and characterization of a nitrogen-doped mesoporous carbon aerogel and its polymer precursor. J Therm Anal Calorim 134(2):933–939. https://doi.org/10.1007/s10973-018-7318-4

46. Shariff AM, Beshir DM, Bustam MA, Maitra S (2010) Some studies on the synthesis and characterization of carbon aerogel. Trans Indian Ceram Soc 69(2):83–88. https://doi.org/10.1080/0371750X.2010.11090822

47. Yan M-F, Zhang L-H, He R, Liu Z-F (2015) Synthesis and characterization of carbon aerogels with different catalysts. J Porous Mater 22(3):699–703. https://doi.org/10.1007/s10934-015-9942-8

48. Imani A, Farzi G, Ltaief A (2013) Facile synthesis and characterization of polypyrrole-multiwalled carbon nanotubes by in situ oxidative polymerization. Int Nano Lett 3(1):52. https://doi.org/10.1186/2228-5326-3-52

49. Cheng Y, Xu P, Zeng W, Ling C, Zhao S, Liao K, Sun Y, Zhou A (2017) Highly hydrophobic and ultralight graphene aerogel as high efficiency oil absorbent material. J Environ Chem Eng 5(2):1957–1963. https://doi.org/10.1016/j.jece.2017.04.005

50. Kraiwattanawong K, Tamon H, Praserthdam P (2011) Influence of solvent species used in solvent exchange for preparation of mesoporous carbon xerogels from resorcinol and formaldehyde via subcritical drying. Microporous Mesoporous Mater 138(1–3):8–16. https://doi.org/10.1016/j.micromeso.2010.10.001

51. Feng J, Feng J, Zhang C (2011) Shrinkage and pore structure in preparation of carbon aerogels. J Sol Gel Sci Technol 59(2):371–380. https://doi.org/10.1007/s10971-011-2514-8

52. Babazadeh M, Rezazad Gohari F, Olad A (2012) Characterization and physical properties investigation of conducting polypyrrole/TiO2 nanocomposites prepared through a one-step "in situ" polymerization method. J Appl Polym Sci 123(4):1922–1927. https://doi.org/10.1002/app.34689

53. Zhu J, Zhang X, Haldolaarachchige N, Wang Q, Luo Z, Ryu J, Young DP, Wei S, Guo Z (2012) Polypyrrole metacomposites with different carbon nanostructures. J Mater Chem 22(11):4996–5005. https://doi.org/10.1039/C2JM14020A

54. Chabi S, Peng C, Yang Z, Xia Y, Zhu Y (2015) Three dimensional (3D) flexible graphene foam/polypyrrole composite: towards highly efficient supercapacitors. RSC Adv 5(6):3999–4008. https://doi.org/10.1039/C4RA13743D

55. You B, Wang L, Yao L, Yang J (2013) Three dimensional N-doped graphene–CNT networks for supercapacitor. ChemComm 49(44):5016–5018. https://doi.org/10.1039/C3CC41949E

56. Chang H-H, Chang C-K, Tsai Y-C, Liao C-S (2012) Electrochemically synthesized graphene/polypyrrole composites and their use in supercapacitor. Carbon 50(6):2331–2336. https://doi.org/10.1016/j.carbon.2012.01.056

57. Fan L-Z, Maier J (2006) High-performance polypyrrole electrode materials for redox supercapacitors. Electrochem commun 8(6):937–940. https://doi.org/10.1016/j.elecom.2006.03.035

58. Memioğlu F, Bayrakçeken A, Öznülüer T, Ak M (2012) Synthesis and characterization of polypyrrole/carbon composite as a catalyst support for fuel cell applications. Int J Hydrog Energy 37(21):16673–16679. https://doi.org/10.1016/j.ijhydene.2012.02.086

59. Chen W-C, Wen T-C, Teng H (2003) Polyaniline-deposited porous carbon electrode for supercapacitor. Electrochim Acta 48(6):641–649. https://doi.org/10.1016/S0013-4686(02)00734-X

60. Lee W-h, Moon JH (2014) Monodispersed N-doped carbon nanospheres for supercapacitor application. ACS Appl Mater Interfaces 6(16):13968–13976. https://doi.org/10.1021/am5033378

61. Zhang D, Dong Q-Q, Wang X, Yan W, Deng W, Shi L-Y (2013) Preparation of a three-dimensional ordered macroporous carbon nanotube/polypyrrole composite for supercapacitors and diffusion modeling. J Phys Chem C 117(40):20446–20455. https://doi.org/10.1021/jp405850w

62. Sun X, Xu Y, Wang J (2012) Electropolymerized composite film of polypyrrole and functionalized multi-walled carbon nanotubes: effect of functionalization time on capacitive performance. J Solid State Electrochem 16(5):1781–1789. https://doi.org/10.1007/s10008-011-1619-x

63. Shi C, Zhitomirsky I (2011) Electrodeposition of composite polypyrrole–carbon nanotube films. Surf Eng 27(9):655–661. https://doi.org/10.1179/1743294410Y.0000000004

64. Gan JK, Lim YS, Pandikumar A, Huang NM, Lim HN (2015) Graphene/polypyrrole-coated carbon nanofiber core–shell architecture electrode for electrochemical capacitors. RSC Adv 5(17):12692–12699. https://doi.org/10.1039/C4RA14922J

65. Xu S, Yang H, Wang K, Wang B, Xu Q (2014) Effect of super-critical CO2 on fabrication of free-standing hierarchical graphene oxide/carbon nanofiber/polypyrrole film and its electrochemical property. Phys Chem Chem Phys 16(16):7350–7357. https://doi.org/10.1039/C3CP54957G

66. Kumar A, Singh RK, Singh HK, Srivastava P, Singh R (2014) Enhanced capacitance and stability of p-toluenesulfonate doped polypyrrole/carbon composite for electrode application in electrochemical capacitors. J Power Sources 246:800–807. https://doi.org/10.1016/j.jpowsour.2013.07.121

67. Bleda-Martínez MJ, Peng C, Zhang S, Chen GZ, Morallón E, Cazorla-Amorós D (2008) Electrochemical methods to enhance the capacitance in activated carbon/polyaniline composites. J Electrochem Soc 155(9):A672. https://doi.org/10.1149/1.2956969